Pergamon

0956-7151(94)E0094-W

Acta metall. mater. Vol. 42, No. 10, pp. 3463–3479, 1994

0956-7151/94 $7.00 + 0.00

A BINARY MODEL OF TEXTILE COMPOSITES—I. FORMULATION

B. N. COX[1], W. C. CARTER[1]† and N. A. FLECK[2]

[1]Rockwell International Science Center, Thousand Oaks, CA 91360, U.S.A. and
[2]Engineering Department, Cambridge University, Cambridge CB2 1PZ, England

(Received 14 January 1994)

Abstract—This paper presents a finite element model of polymer composites with three-dimensional (3D) reinforcement. The model performs Monte Carlo simulations of failure under monotonic and fatigue loading. The formulation of the model is guided by extensive prior experimental observations of 3D woven composites. Special emphasis is placed on realistic representation of the pattern of reinforcing tows, random irregularity in tow positioning, randomness of the strengths of constituent elements, and the mechanics of stress redistribution around sites of local failure. The constitutive properties of model elements (or their distributions) are based on micromechanical models of observed failure events. Material properties that are appropriately analyzed by the model are contrasted with those amenable to much simpler models. Some illustrative model simulations are presented. Prescriptions for the calibration of the model for design and reliability applications and details of its performance in simulating the elastic and damaged regimes of 3D woven composites will appear in subsequent papers.

1. INTRODUCTION

Elsewhere [1–4], detailed observations have been reported of the mechanisms of failure of three-dimensional (3D) woven polymer composites in monotonic and cyclic tension, compression and bending. The failure mechanisms depend on the architecture of the reinforcement and irregularity in its deployment. The irregularity may arise during the weaving process or during subsequent consolidation with resin. It typically consists of waviness in nominally straight tows due to lateral pressure from their neighbors or concertina deformations due to compression during processing. Irregularity usually has a modest effect on average elastic moduli but a strong effect on strength. Both irregularity and certain topological features of the reinforcement may be regarded as random geometrical flaws. Broad distributions of these flaws in space and strength favor noncatastrophic modes of failure, large strain to failure, damage tolerance, and notch insensitivity [1, 2]. These favorable properties are also enhanced in common 3D woven composites by the coarseness of the reinforcement: larger tow cross-sections lead to longer zones of slip around tows near sites of tow failure, which favors notch and damage insensitivity [2].

Thus understanding the engineering properties of 3D composites, including unnotched strength, notch sensitivity, and delamination resistance, requires detailed modeling of the random variations in load distribution throughout the composite. A successful model must persist beyond the elastic regime to consider load redistribution as the composite progressively fails. This paper seeks the *simplest possible* formulation of such a computational model.

The essence of the model is a division of the composite into a binary system comprising "tow" elements, which represent axial tow properties only, and solid "effective medium" elements, which account for other mechanical properties. Explicit account of the reinforcement architecture is ensured by defining the two elements to have the same topology as the tows in the actual composite. The constitutive laws of tow and effective medium elements are derived by micromechanical models of the experimentally observed local failure events. They contain random parameters corresponding to irregularity in the reinforcement geometry or in the mechanical properties of the constituent materials.

This paper reviews the experimental observations that underpin the model and lays out the micromechanical models of local failure events that are used to generate the constitutive laws. Reference [5] and subsequent papers will address the question of which model parameters can be regarded as known *a priori* and which must be determined by calibrating experiments.

2. EXPERIMENTAL BACKGROUND

The materials studied in prior work [1–3] were angle or orthogonal interlock weaves of carbon fiber tows, impregnated and consolidated with epoxy resins. The tows comprise straight warp tows known as "stuffers", straight weft tows known as "fillers", and oscillating warp tows known as "warp weavers".

†Present address: National Institute of Standards Technology, Gaithersburg, MD 23344, U.S.A.

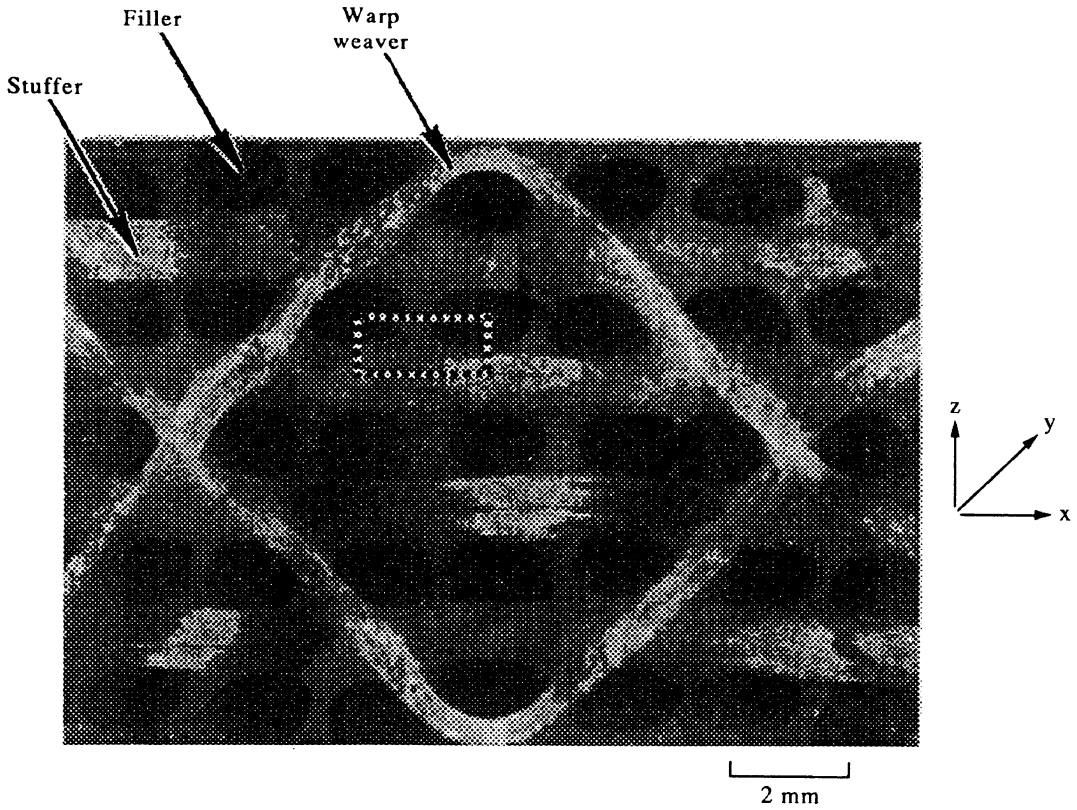

Fig. 1. A section of a through-the-thickness angle interlock woven composite, consisting of AS4 carbon tows in an epoxy resin matrix (from [1]). The rectangle outlines one face of a typical effective medium element.

(In a few cases studied, the warp weavers were glass fiber tows.) The stuffers and fillers form a coarse 0°/90° laminate, while the warp weavers provide through-thickness reinforcement. One particular case is illustrated in Fig. 1. While there are few limitations in principle on weave architecture or tow denier†, weaving costs generally restrict stuffers and fillers to be at least ~5 k denier and usually 10–15 k denier. This implies a tow cross-sectional area of ~1 mm, and in sheet applications in which normal pressure is used during processing to maximize fiber volume fraction, a typical 5 mm thick panel might contain between 9 and 15 layers of stuffers and fillers‡. The reinforcing tows remain distinct during consolidation and are easily identified in the composite. Further description of interlock weaves appears in [1–5] and below.

The discreteness of tows is fundamentally important in failure. When a tow fails locally, whether in tension, compression or fatigue, the damage generally extends over its whole cross-section, but does not necessarily extend to neighboring tows. Furthermore, other than at the site of failure, a failed tow generally remains intact, frequently debonding§ from the surrounding composite and displacing axially relative to it as one body.

The following summary refers to uniaxial experiments in which the load was aligned with the stuffers. Observations for loads aligned with the fillers and for bending experiments are qualitatively the same.

2.1. *Monotonic loading*

2.1.1. Compression. In compression, some degree of delaminativon between layers of stuffers and fillers nearly always occurs. If the through-thickness reinforcement is absent or rendered ineffective by crimping during consolidation, delamination cracks can run the length of the specimen [2]. Premature failure with brittle stress/strain characteristics then ensues via Euler buckling of one or more delaminated layers. If, on the other hand and as surely preferred in structural applications, the through-thickness reinforcement is properly designed and unimpaired in processing, delamination cracks remain limited in length and associated buckling may be suppressed altogether.

For this more desirable case, stress–strain curves in uniaxial compression for dogbone specimens of angle

†Denier measures the mass in grams of 9000 m of yarn.
‡In an interlock weave, the number of layers of stuffers and fillers is usually odd, since fillers are the outermost straight tows on both sides of the stack (e.g. Fig. 1).
§The term debond crack refers throughout this paper to a crack lying entirely within the resin, but circumscribing a tow and detaching it from the surrounding composite. Debonding of individual graphite or glass fibers from the resin has not been observed in any of the materials under discussion.

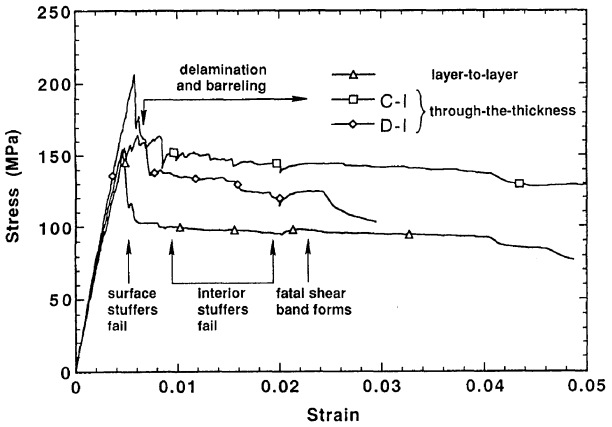

Fig. 2. Regimes of the stress–strain history where various failure mechanisms operate in angle interlock weaves under uniaxial compression (from [1]).

interlock composites are typified by those in Fig. 2. While considerable variations in strength and strain to failure are found for specimens of different loading geometry or interlock weaves of different architecture or processing history [1, 2], the principal events indicated in Fig. 2 and the approximate domains of strain with which they are associated are those found generally.

The first significant nonlinearity usually occurs at loads exceeding half the peak load. It arises from microbuckling of nominally aligned tows, i.e. stuffers in the experiments being summarized here, and some matrix microcracking. Moiré interferometry reveals soft spots in the composite at locations where the misalignment of a stuffer is unusually severe [1].

Around the peak load, a sequence of pronounced load drops occurs. Limited delaminations may cause some of these, but many correspond to the formation of kink bands in stuffers. When revealed by sectioning after ultimate failure at high strains, the kink bands generally exhibit quite complex configurations of internal damage. Figure 3 shows a typical case. Several distinct kink bands can be seen, lying adjacent to one another. Further remarks on the formation of such nests of kink bands and their implications for constitutive laws appear below. Acoustic events during tests and sectioning post-mortem indicate that kink bands are formed continually over a fairly wide range of strains as marked in Fig. 2, with the exact range depending on the material and the test configuration.

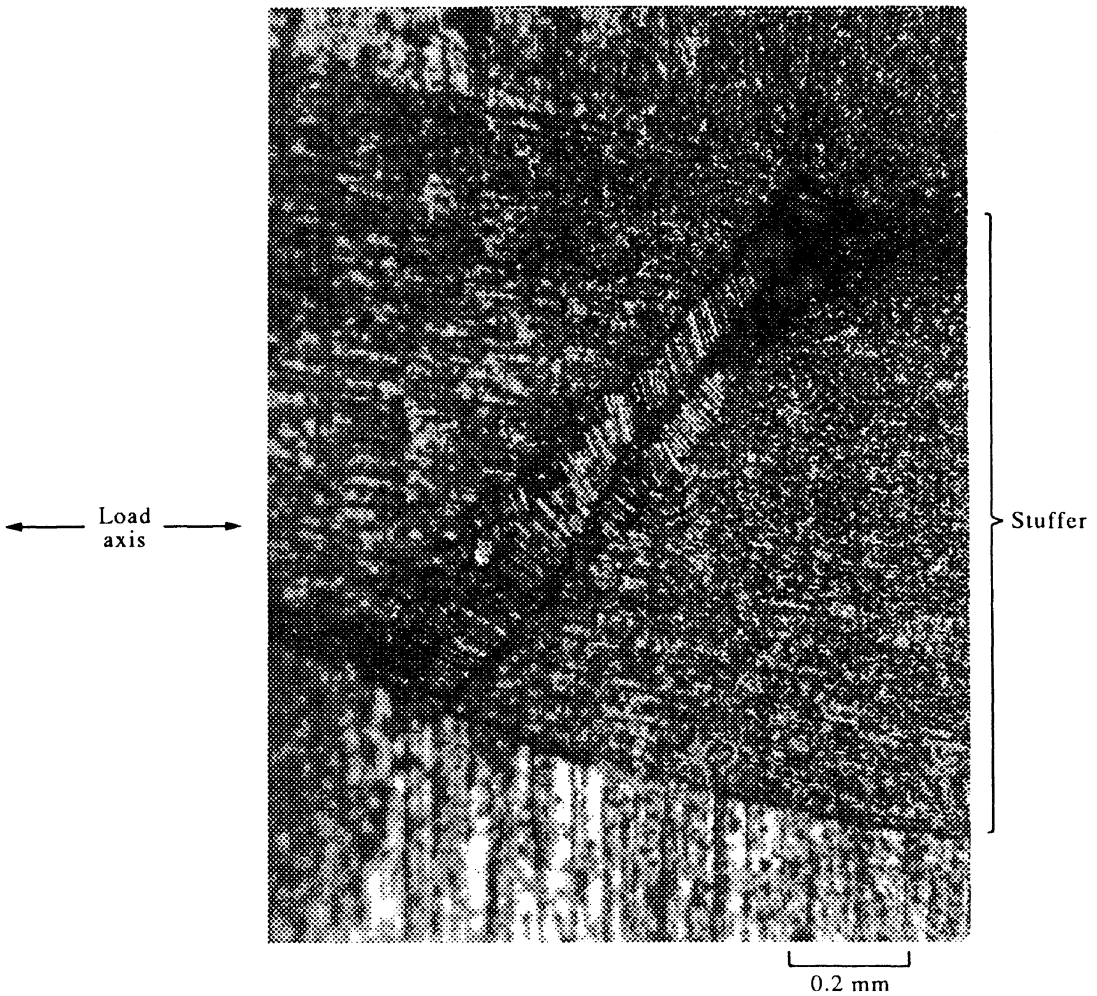

Fig. 3. System of kink bands at one site of local failure in a woven interlock composite tested to failure in uniaxial compression.

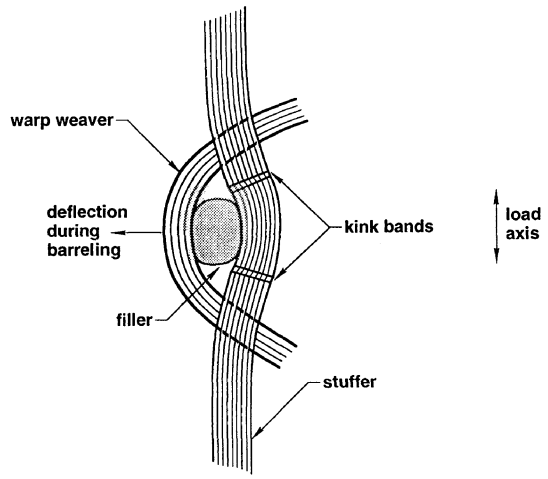

Fig. 4. A common association of kink bands with a particular configuration of tows. In such configurations, the nominally straight stuffer is often distorted as shown [2]. However, kink bands are also found in this configuration even when the stuffer is undistorted.

Kink bands are frequently found in stuffers at sites where a warp weaver wraps around a filler adjacent to the stuffer, as illustrated schematically in Fig. 4. One explanation of this correlation is that the arrangement of tows in Fig. 4 often causes distortions of the stuffer during either weaving or consolidation [2]. The resulting misalignment in the stuffer is usually maximum in the locations where kink bands are found (e.g. Fig. 4). However, some kink bands have been observed in stuffers in the configuration of Fig. 4 that were not substantially misaligned. In such cases, delamination has a crucial role. Delamination cracks, although limited in spatial extent, nevertheless separate the specimen into laminae, which buckle and deflect in directions normal to both fillers and

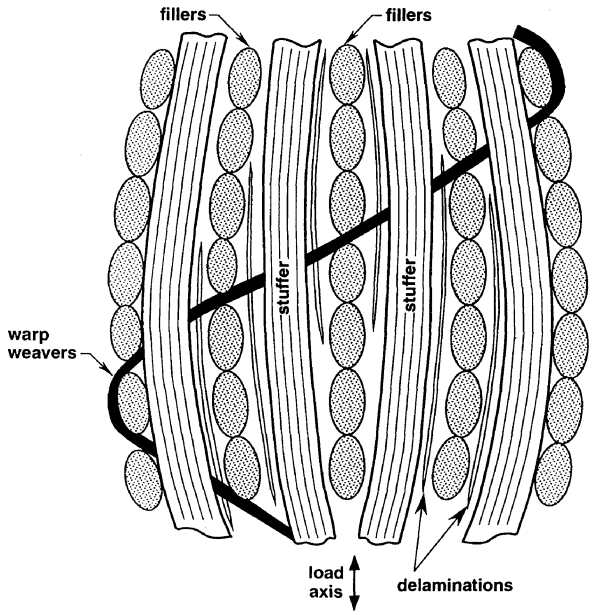

Fig. 5. Schematic of delamination and barreling in a through-the-thickness angle interlock composite under uniaxial compression.

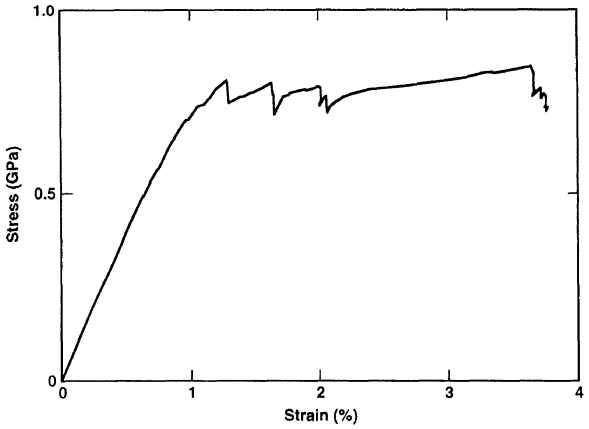

Fig. 6. Typical stress–strain curve of a 3D interlock woven composite under uniaxial tension (from [2]).

stuffers, causing the specimen to barrel (Fig. 5) [1]. Where the barreling deflection is opposed by a warp weaver, as in Fig. 4, a filler is compressed into a stuffer, lowering the critical stress for its kinking. Delamination and barreling typically influence kink band formation and the overall stiffness of the composite over the range of strains indicated in Fig. 2 [1].

For kink band mediated failure, the sequence of events leading to ultimate failure varies with material and specimen configuration. Generally speaking, it consists of some fatal configuration of kink bands and associated matrix failure; although the matrix contributes little directly to strength. In the tests of Fig. 2, ultimate failure is associated with a localized macroscopic shear band, along which all stuffers have failed by kinking. However, this shear band is not manifest in photographic records of the test specimens until compressive strains between 2 and 4% have been applied. Post mortem sectioning in these cases reveals widespread kink bands on stuffers lying at or near specimen surfaces, which presumably anteceded those on the fatal shear band. Cuboidal specimens of composites with relatively low total fiber volume fractions commonly fail without kink bands ever localizing into a shear band, being distributed instead over the entire specimen, whether in near-surface or interior regions [1]. At the other extreme, tests of interlock composites with high total fiber volume fractions (achieved by high pressure during consolidation) occasionally end with nearly all kink bands lying on a fatal shear band [2]. *The extent to which kink bands are delocalized corresponds with the strain to failure for tests under displacement control.*

2.1.2. Tension. Data for 3D interlock woven composites under uniaxial tension were presented in [2]. A representative stress–strain curve for a composite with high total fiber volume fraction is reproduced in Fig. 6. The principal damage events observed during such a test are matrix cracking (both tensile and delamination), the rupture of individual tows, and tow pullout. The last two are clearly visible in the typical specimen of Fig. 7 (from [2]). Tow pullout is

the source of the exceptionally high strain to ultimate failure suggested by Fig. 6.

As in compression tests, some nonlinearity may arise prior to peak load from the straightening under load of initially misaligned stuffers, although simple estimates suggest this should be small (see Section 4). Most softening in the pre-peak load regime is caused by matrix cracking normal to the load axis, especially in the matrix between fillers [2]. As in compression, discrete load drops are often seen around peak load, but in tension both these and the peak load are manifestations of tow rupture. As stuffers continue to rupture, the matrix cracks between fillers extend and coalesce into a large "tension crack" such as that depicted in Fig. 7. The tension crack (or occasionally a sequence of offset tension cracks linked by delaminations) develops into the fatal failure mechanism [2]. Final failure is delayed by extensive tow pullout across the expanding tension crack. Tow pullout distances in tension are typically several millimeters, while in some cases they exceed 10 mm.

2.1.3. Stress redistribution. Kink band formation or tensile rupture of an individual tow is generally accompanied by debonding of the tow from the surrounding composite. The debonding typically extends several millimeters along the tow from the failure site. Such large slip lengths provide excellent relief of stress concentration around the failure site, with an implied tendency for noncatastrophic failure. The large slip lengths are a direct consequence of the coarseness of the woven reinforcement. They rise in proportion to the tow diameter [2].

2.2. Fatigue

2.2.1. Compression–compression. As in monotonic loading, ultimate failure in 3D woven composites in compression–compression fatigue is the sum of many kink band failures in individual stuffers. In contrast with the damage sequence under monotonic loading, kink band formation in fatigue is the first observable damage and causes rather than ensues from matrix damage [3]. This has led to the inference that fatigue damage accumulates within tows, most likely as deterioration of the resin. As in monotonic compression, kink bands in fatigue occur first at locations where stuffers are most misaligned with respect to the load axis or lateral loads originating in warp weavers might be expected (Fig. 8). Such observations are consistent with earlier work on the influence of misalignment in the fatigue of unidirectional composites [6, 7].

2.2.2. Tension–tension and tension–compression The progression of damage under tension–tension or fully reversed loading is distinguished from that in compression–compression fatigue by the relatively early appearance of matrix cracks normal to the applied load axis [3]. These microcracks increase in density with cycles and occur at tensile amplitudes in the elastic regime of monotonic tension data.

Although the matrix cracks cause a modest increase in specimen compliance, ultimate failure is the result of tow rupture. Neither is there any evidence that the matrix cracking directly induces tow failure. Instead, it would appear that just as in compression–compression fatigue, tow rupture in tension

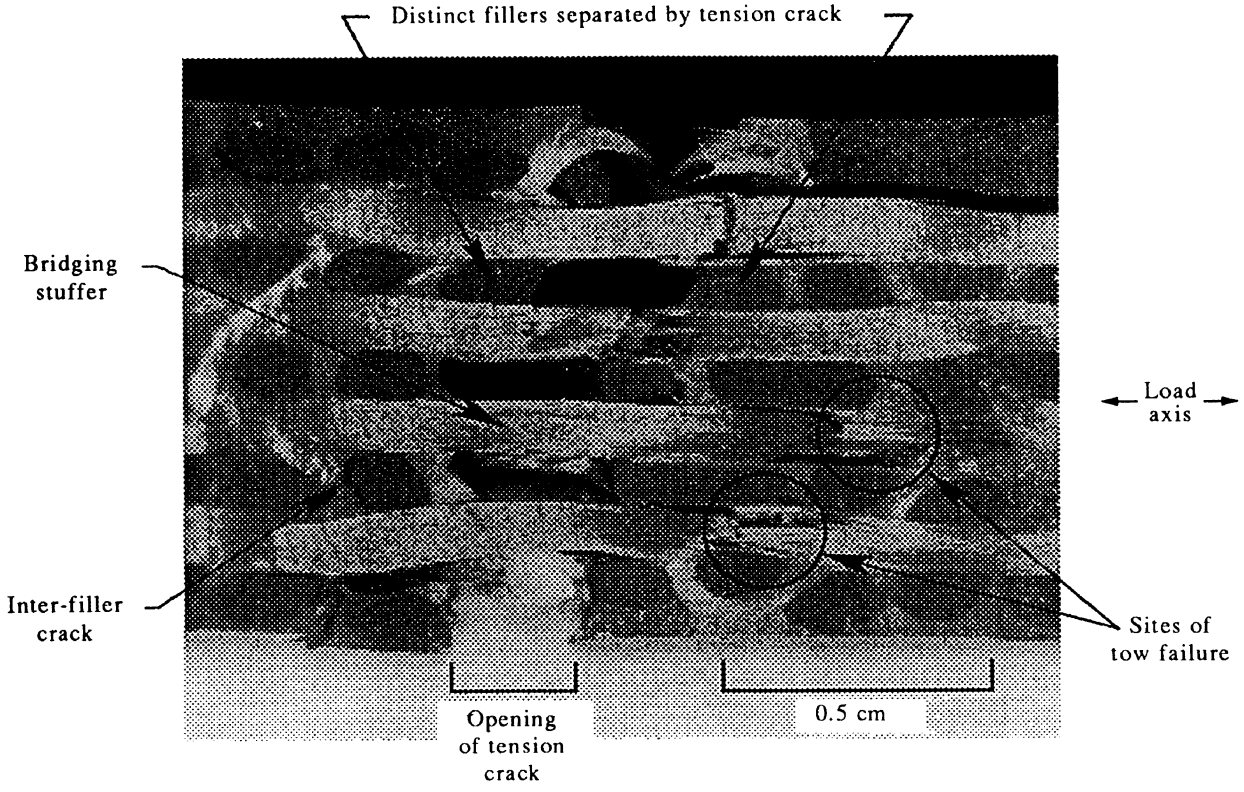

Fig. 7. A through-the-thickness angle interlock specimen after testing in uniaxial monotonic tension.

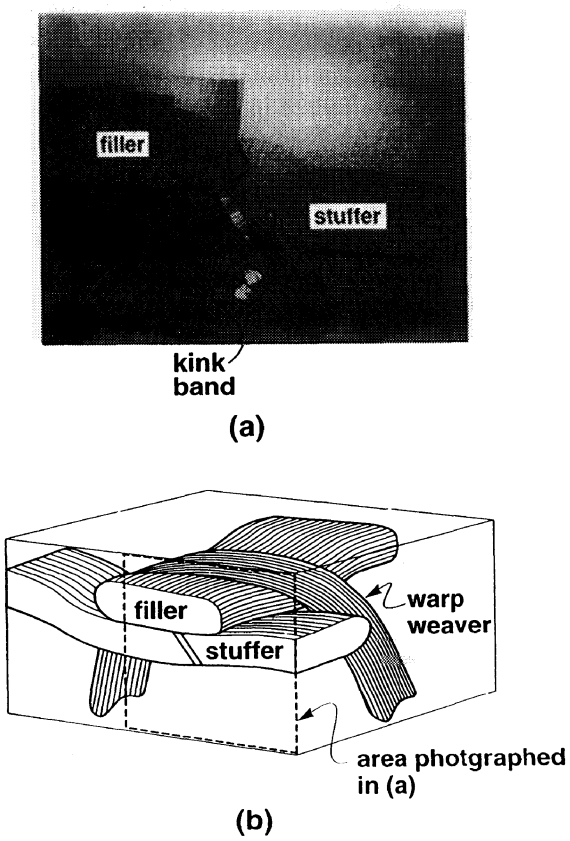

Fig. 8. (a) A kink band found after a runout compression–compression fatigue test in an angle interlock composite [3]. (b) Schematic of deformation of the stuffer and filler in (a) by a warp weaver pressed into them during either weaving or consolidation.

signals the maturation of degradation that is internal to the load bearing tows. There is again correlation between sites of rupture and misalignment.

3. MODELS APPROPRIATE TO DIFFERENT ASPECTS OF COMPOSITE BEHAVIOR

The experiments reported in [1–4] and elsewhere suggest that the mechanical properties of 3D composites can be separated into two categories: those that can be predicted to within experimental scatter by elementary models; and those that cannot. Table 1 summarizes this classification.

3.1. Problems for which the Binary Model is not required

Flat panels consisting of a single weave type behave as orthotropic bodies in the elastic regime. Elastic constants are well approximated by combining rules of mixtures or other simple models of unidirectional composites with standard laminate theory and some crude estimates of the softening effects of tow irregularity [2, 8] (see also earlier references cited in [8]).

Unnotched strength in tension can be estimated from the strength quoted for pristine fibers by the manufacturer, corrected for volume fractions [2]. Unnotched strength in compression is governed by the mechanics of kink band formation. In the absence of lateral loads, the critical stress, σ_k, for the initiation of a kink band is related simply to the shear flow stress in the matrix, τ_0, and the misalignment, ϕ_k, of the fibers with respect to the applied load axis [9, 10]

$$\sigma_k = \tau_0/\phi_k. \quad (1)$$

To a good approximation in most polymer composites, σ_k does not depend on the fiber modulus [11]. Reasonable estimates of unnotched compressive strength then follow from values of τ_0 measured in independent tests on $\pm 45°$ laminates and the distribution of ϕ_k deduced from optically scanned sections of woven composites [2].

The extent of fiber pullout observed in unnotched tension tests (e.g. Figs 6 and 7) suggests that notch sensitivity in tension should be modeled via a cohesive zone of damage extending from any stress concentrator [2]. Within the cohesive zone, the mechanics of tow pullout will govern the relation $p(u)$ between the bridging tractions, p, acting across the damage zone and the displacement discontinuity, $2u$ (or crack opening displacement, u). In [2], the characteristic cohesive zone length, l_{ch}, was shown to be to order of magnitude 0.1–0.5 m. The function $p(u)$ can be deduced directly from measurements of force and displacement on unnotched tensile specimens, as long as the specimen width is much less than l_{ch}, e.g. ~ 10 mm. Once $p(u)$ is known, notch sensitivity and the influence of part size and geometry on strength can be computed from the relatively simple and well developed fracture mechanics of cohesive zones or bridged cracks.

Delamination and subsequent buckling under monotonic compression, the primary mechanism of

Table 1. Predicting the properties of 3D composites

(i) Some properties predicted by simple models	
Property	Model
Stiffness of flat coupons	Rule of mixtures/mean field models Laminate theory Rough estimates of the effects of tow irregularity
Unnotched strength for aligned loads	Compression: criterion for kink band formation Tension: tow rupture strength
Notch sensitivity/fracture toughness in tension	Cohesive zone model
Delamination and buckling	Beams or plates on an elastic foundation
(ii) Some problems requiring a computational model (the Binary Model)	
Problem	Remarks
Stiffness/strength of integral structures	Require stress distribution in tows in complicated arrangements
Progression of damage in monotonic loading and fatigue Localization/delocalization of damage Open-hole compression Fatigue near stress concentrators Constitutive law for cohesive zone in tension	Depend on local stress distributions, distributions of flaws, and load redistribution following local failure—stochastic problem

failure against which 3D reinforcement has been introduced into polymer composites, can also be modeled relatively simply. The delamination problem can be modeled by a variant of existing laminate theories in which elastic springs couple separable laminae (e.g. [12]). For 3D composites, the springs represent the through-thickness reinforcement. The problem of buckling of delaminated layers in 3D composites can be described as that of classical buckling plates on an elastic foundation [13, 14].

For nearly all of the above properties, the 3D composite behaves essentially as a laminate of homogeneous layers. The effects of the 3D weave or of irregularity in tow positioning are either small or are determined by averages over large volumes of material. The sole exception is modeling based on the concept of a cohesive zone, for which the crucial relation $p(u)$ depends strongly on the irregularity and geometrical details of the reinforcement (see [2] and below). However, engineering predictions based on the cohesive zone model can be completed by determining $p(u)$ experimentally; for this particular purpose, the micromechanics underlying $p(u)$ need not be modeled in detail (e.g., [15, 16]).

3.2. Problems to be solved by the Binary Model

Other important problems defy such relatively simple modeling. They are generally those in which macroscopic behavior depends on the details of load distribution throughout the composite. Some examples are given in part (ii) of Table 1.

One very important application of 3D composites is the fabrication of integral structures. Two examples from weaving technology are integral box beams, containing predominantly axial yarns (stuffers) in the upper and lower surfaces, with $\pm 45^\circ$ yarns (warp weavers) in the sides [17]; and integrally woven skin/stiffener panels (e.g. [18]). Because of the complex reinforcement architecture in such structures, laminate models are unlikely to be reliable even in the elastic regime, especially at critical junction regions such as where two sides of a box beam or a stiffener and skin merge. Predictions of stiffness and strength require the calculation of loads in geometrically complex arrangements of tows.

While the effects of complex tow arrangements present a deterministic problem, several other aspects of composite behavior depend on how random flaws are distributed in both strength and space. These properties demand a stochastic model.

In compression, the more misaligned segments of tows will fail by kink band formation at lower values of the local axial stress, following equation (1). If lateral loads also act on a tow as from tow wrap-around, an additional shear stress, τ_l, is induced. For the simplest assumptions concerning local fiber and kink band geometry, σ_k is lowered further according to [10]

$$\sigma_k = [\tau_0 - \tau_l]/\phi_k. \tag{2}$$

The tensile rupture of tows has not been quantitatively modeled. However, it seems plausible that segments of tows that are unusually bent, squashed, or subjected to lateral loads will have reduced tensile strength.

In both compression and tension, fluctuations in tow alignment also affect the onset of nonlinearity by causing uneven load distribution. A tow segment with unusually high waviness is more compliant under axial loading than one that is already straight. Straighter tow segments will therefore bear a disproportionate share of the load and tend to fail early in loading.

Thus the onset of damage, whether under monotonic or cyclic loading, must depend on the distribution of flaw strengths and the evenness of load distribution. The progression of damage at higher strains will depend on both of these factors as well as the way loads are redistributed around a local failure event. In both compression and tension, load redistribution around a kinked or ruptured tow is mediated by friction acting around the periphery of the broken tow [2]. The critical stress for frictional sliding dictates the distance along the failed tow over which the tow is reloaded to far field loads by load transfer, and it therefore dictates the range of interaction of flaws.

One important characteristic of damage progression is whether successive local failure events form a localized band of macroscopic damage or whether they are delocalized and widely distributed over the gauge section. A transition from localized to delocalized damage, manifested as a brittle–ductile transition in compressive stress–strain curves, has already been noted for 3D stitched and woven composites [1, 2]. A qualitative account of this transition can be found in [1, 2]. Quantitative analysis requires the Binary Model, with an appropriately detailed solution of the statistics of local failure events and load redistribution. Modeling the transition from localized to delocalized damage is the key to modeling strain to failure and damage tolerance.

While predictions of notch sensitivity in tension can be made using an empirically determined constitutive law, $p(u)$, in a cohesive zone model, composite design requires understanding how $p(u)$ is determined by microstructure. Tow pullout lengths are determined partly by the flaw distribution within tows, wider distributions favoring long pullout lengths (e.g. [19, 20]). Pertinent flaws comprise both intrinsic strength variations and geometrical irregularities, especially locations where cross tows might impose weakening lateral loads on an aligned tow. Pullout loads are also influenced by transverse compression experienced by ruptured tows, since pullout is resisted by friction. Transverse compression can be strongly enhanced by through-thickness tows, which often survive the rupture of neighboring axial tows, by the mechanism illustrated in Fig. 9. Computing

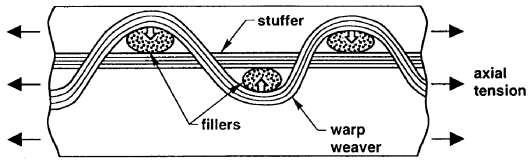

Fig. 9. Schematic of the development of transverse compression by warp weavers during tensile loading. White arrows indicate the sense of loads imposed on neighboring tows by warp weavers, which tend to straighten when strained in the direction of the load. The case shown is a layer-to-layer angle interlock weave.

how all these factors of reinforcement architecture and irregularity influence $p(u)$ is another application of the Binary Model.

The likely success of cohesive zone models for predicting notch sensitivity in tension is due to the large values estimated for the characteristic cohesive zone length, l_{ch}. Since damage is spread over such large lengths before failure, details of the tow geometry near the stress concentration have minimal effect. Stochastic quantities are sensed only in their averages over the cohesive zone. In compressive loading or cyclic loading, where tow pullout lengths may not be as large as in monotonic tension, the failure process could depend much more critically on events confined to a relatively small volume near a stress concentrator—perhaps containing only a few tows. If experiments show such behavior (they are in progress), the Binary Model will be required to compute the effects of notch shape, tow positioning, and random geometrical flaws.

4. BINARY MODEL OF A 3D COMPOSITE

The Binary Model is a finite element model, in which the highly anisotropic and heterogeneous structure of a 3D composite is resolved into simple constituents: reinforcing "tows", which primarily represent the axial properties of individual tows; and an "effective medium", which represents all other properties of the tows, resin pockets, voids, etc. in an average sense. The usefulness of this division rests on the fact that the axial modulus of the reinforcing fibers, whether graphite, glass or other material, is generally two orders of magnitude greater than the modulus of the resin. The axial modulus of the fibers dominates strength and stiffness under aligned loads, while the modulus of the resin dominates properties that depend on the effective medium, notably the shear and transverse stiffnesses and Poisson's effect. When the model is discretized, the tows are divided into two-noded line elements possessing axial rigidity only, with no prescribed shear or bending resistance. The effective medium is divided into solid elements, which, at least in the elastic regime, can often be considered homogeneous and isotropic. The effective medium elements and the tow elements are coupled by imposing constraints between certain nodes of each. The constraint will usually comprise an undamaged state, in which the nodes simply share the same coordinates, and a damaged state, allowing some relative displacement. As in the real composite, no two reinforcing tows are coupled directly. They interact only via the effective medium. Tow and effective medium elements are commensurate with the characteristic scale of the reinforcement architecture, e.g. the distance between points at which one tow crosses two other tows successively. Relatively large sections of the composite structure can thus be modeled in a calculation with a modest number of degrees of freedom.

Both tow and effective medium elements are nonlinear, with plasticity and local failure incorporated in their assigned constitutive properties. The constitutive laws for tow and effective medium elements also embody stochastic parameters.

Figure 10 shows a typical arrangement of nodes on tow and effective medium elements in a small volume of a layer-to-layer angle interlock woven composite. In this particular architecture, stuffers and fillers lie in orthogonal layers, while warp weavers supply through-thickness reinforcement by looping above and below individual fillers in adjacent filler layers. This structure lends itself to the cuboidal effective medium elements exemplified by the shaded volume in Fig. 10.

As in any discretization of a continuous (or piecewise continuous) body, there is some arbitrariness in the choice of element size. The choice illustrated in Fig. 10 entails the minimum density of tow nodes required to reproduce the topology of the reinforcement faithfully. A higher density of nodes could be chosen, but that would betray the spirit of finding the *simplest possible* realistic formulation. Nevertheless, as well as the assurance of computational precision in modeling tows, other physical conditions must also

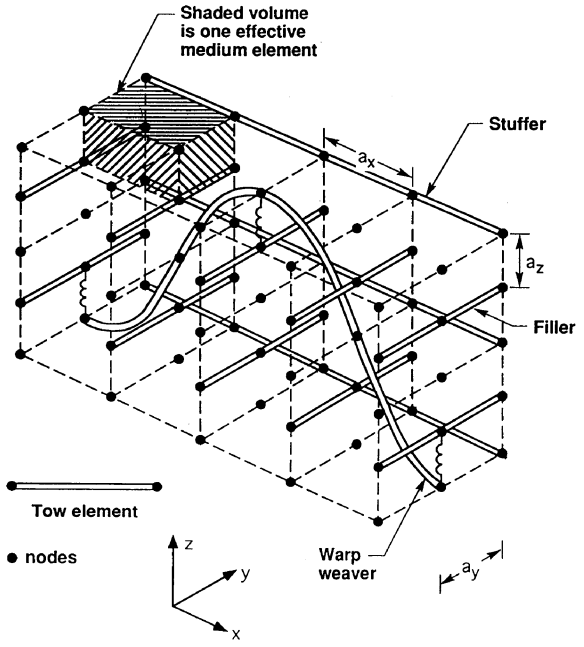

Fig. 10. Tow and matrix elements in a layer-to-layer angle interlock woven composite.

be met in choosing the element size. These will be discussed below.

Once the element size has been chosen, the length scale it introduces determines the way geometrical fluctuations are treated. Thus, the irregularity of a tow that undulates over wavelengths larger than the element size can be mimicked simply by displacing appropriate nodes on that tow in the initial, load-free configuration of the model. If a geometrical property fluctuates over a length less than the element size, the variation must be incorporated in the constitutive law provided for that element. Some explicit examples of this will be given below.

The conceptual division of the composite into tow and effective medium elements is ultimately a matter of convenience. The end product is a nonlinear finite element model, which must be equivalent to a model containing only solid elements, with the effects of the tow elements incorporated in appropriate anisotropic and nonlinear constitutive laws. However, the geometrical complexity of the reinforcement would oblige the definition of many different types of solid element in such a model, depending on the local tow configuration. Furthermore, the treatment of stress redistribution around a failed tow and the computation of local axial stresses in tows would be cumbersome.

4.1. Constitutive laws for tow elements

The properties of tow elements follow from elementary arguments.

4.1.1. Elastic properties. The axial elastic modulus, E_t, of a tow that is initially straight can be estimated by the rule of mixtures

$$E_t = V_t E_f + (1 - V_t)E_r \tag{3}$$

where V_t is the volume fraction of fibers within a single tow and E_f and E_r are Young's moduli for the fibers and resin, the former measured axially. The axial stiffness, k_t, of the corresponding tow element in the binary model is given by

$$k_t = (E_t - E_m)A_t \tag{4}$$

where A_t is the tow's cross-sectional area and E_m is Young's modulus for the effective medium (specified below). The subtraction of E_m in defining k_t avoids double counting that would arise because the effective medium elements fill all space. The area A_t is deducible from the length per unit mass, y, of the tow (known as the "yield"); the density, ρ_f, of the fibers; and V_t according to

$$A_t = \frac{1}{V_t \rho_f y}. \tag{5}$$

If the tow is undulating initially, its response to axial loads σ_t can be described by the differential axial displacement, u, between two points separated by some gauge length L

$$u = L\sigma_t/E_t + L\epsilon_u \equiv L\epsilon \tag{6}$$

where ϵ_u is a strain contribution arising from straightening of the undulations. If the tow undulates over periods greater than the element size, both of these terms will be computed as part of the solution of the discretized model, with tow undulations entered explicitly as initial nodal offsets. However, if the tow undulates over periods less than the element size, the second term in equation (6) must be computed in advance by micromechanical modeling. The tow elements then possess a possibly strain-dependent, reduced effective axial stiffness, $E_e = d\sigma_t/d\epsilon$.

Calculating E_e accurately is difficult. However, knockdowns due to waviness or irregularity should never lower the composite modulus by more than 10–20%: if they do, the composite is either poorly designed or badly fabricated. Experimentally measured scatter in the macroscopic composite modulus is usually 5–10% in 3D woven or braided composites [1, 2, 21], while tow waviness itself is difficult to characterize and its statistics difficult to measure. Therefore, it is unlikely to be profitable to employ more than rough estimates for E_e. More usefully, simple models of the effects of tow waviness or irregularity allow competing composite designs to be compared or the effects of irregularity induced by processing to be estimated. The details of this idea are deferred to [5, 8]. In the meantime, E_e is simply written

$$E_e = \chi E_t \tag{7}$$

where χ is a random variable for the tow elements in a single simulation and typically $\chi \gtrsim 0.9$.

For large strains, equation (7) will generally be nonlinear: an undulating tow will stiffen as it straightens. However, in most applications, it will be valid to assume that the knockdown factor χ is independent of strain. At strains high enough for tow straightening to change E_e, the composite stress–strain relation is likely to be dominated by tow and matrix failures.

In assigning the resistance of tows to lateral deflections to the stiffness of the effective medium, it is assumed that such deflections would arise from shear alone. However, at least in principle, both shear and pure bending could contribute significantly to lateral deflections. The proportions of the total deflection arising from each will depend on the length of the tow element, among other things, with long elements favoring the dominance of the pure bending contribution. A simple estimate of these effects is presented in Appendix A. *The upshot is that for the computational tow elements defined here and for all current applications in polymer composites, shear is the dominant mode of lateral deflection.* Thus shear stiffness is properly ascribed to the effective medium, leaving the tow elements themselves with no inherent resistance to lateral loads. This division has the added virtue of minimizing the degrees of freedom in the model.

4.1.2. Strength in compression. The strength of a tow in compression is indicated by the mechanics of kink band formation, with the critical value, σ_k, of

the axial stress being given by equation (2). Thus σ_k depends on two factors, the misalignment angle ϕ_k and the local shear stress due to lateral loads, τ_l, both of which change as the composite responds to load. The shear stress, τ_l, in any tow element can be computed at each load increment from the shear in adjoining effective medium elements.

How the misalignment angle ϕ_k is treated depends on whether the misalignment occurs over a gauge length that is larger or smaller than the tow element size. If it is larger, then ϕ_k is computed from the nodal displacements. If smaller, then the role of ϕ_k is subsumed in the constitutive properties of the tow, which are prescribed *a priori* from micromechanical arguments. Misalignments can be measured from digitized photographs of specimen cross-sections, as described in [4, 8]: the inferred ϕ_k will generally be a random variable.

4.1.3. Strength in tension. The stress σ_t in any tow element can be strongly affected by tow undulations. For undulations of wavelength greater than the element length, resulting variations in σ_t are computed directly in solving the model. Undulations lying within a single element are represented by the reduced effective stiffness, E_e, of equation (7): thus

$$\sigma_t = E_e \epsilon_t \tag{8}$$

where ϵ_t is the axial strain in the tow element implied by its nodal displacements alone.

The failure of a tow in tension is modeled simply by the criterion that failure occurs when

$$\sigma_t = \sigma_t^{(c)} \tag{9}$$

where σ_t is the axial stress in the tow element and the critical stress, $\sigma_t^{(c)}$, is a material property. The critical stress depends upon intrinsic flaws in the tow, including flaws associated with crimping or distortion caused by consolidation. It is a random variable whose distribution of initial values will probably always be evaluated by fitting the model to experimental data. As discussed in [2] and Section 3, it may also be reduced during loading by lateral loads imposed on a nominally aligned tow by neighboring tows. If so, the value of $\sigma_t^{(c)}$ for elements in the aligned tow could be lowered during a simulation in proportion to such lateral loads, as measured by the maximum shear in adjacent effective medium elements.

4.1.4. Post-failure properties. The most important local phenomenon following failure of a tow in either compression or tension is the transfer of load to neighboring tows. This is represented by the constitutive law coupling tow and effective medium nodes, as described in the following section. Once the tow has failed, the stiffness of the failed element is usually reduced to zero.

However, there are circumstances where experimental evidence indicates more complex behavior. One is intimated by the complex kink band structure of Fig. 3. Kink bands begin forming at strains of

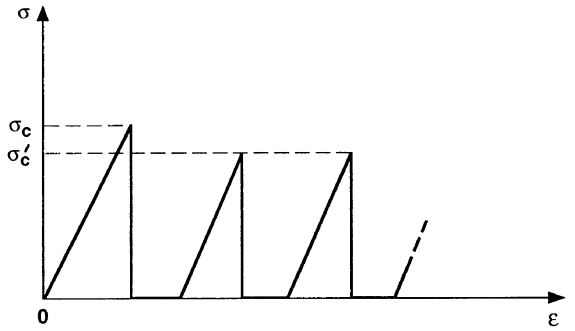

Fig. 11. Schematic of the stress–strain history of a tow element within which multiple kink banding occurs in compression.

1–2%, whereas failure in tests occurs at strains up to 15% [1–3], whereupon post mortem examination is undertaken. Multiple kinks, such as those in Fig. 3, have presumably developed as a succession of kinking events over such large strains. One explanation of this phenomenon is that kinks lock up after a certain amount of axial strain, whereupon the tow can again bear large loads. Further loading can lead to a new kink band, which is very likely to abut the prior damage, which will act as a nucleation site. The mechanics of lockup and its relation to axial sliding of a failed tow are described in Appendix B. The upshot is the schematic stress–strain response for the tow element shown in Fig. 11.

4.1.5. Properties in fatigue. The observed absence of microcracking prior to kink band formation in compression–compression fatigue (Section 2.2) implies that fatigue damage in compression consists of degradation of the interior of the primary load bearing tows. It has previously been pointed out [7] that fiber misalignment causes lateral or resolved shear loads in unidirectional composites that are large enough to damage the epoxy resin. In compressive fatigue loading, such damage will gradually lower the effective shear strength of the resin, which in turn will lower the critical stress for kink band failure [equation (1)]. When that stress falls below the maximum applied compressive stress, the tow will fail. This model is consistent with the observation that kink bands form earliest in fatigue at locations of maximum misalignment. A feasible constitutive law for compressive fatigue is that

$$\frac{d\tau_0}{dN} = -A_1(\Delta\sigma_1 \phi_k)^{n_1} \quad (A_1 > 0), \tag{10}$$

where N is the number of elapsed fatigue cycles, $\Delta\sigma_t$ the local stress amplitude in a tow element whose misalignment is ϕ_k, and A_1 and n_1 are to be evaluated empirically. The exponent n_1 could be deduced from the slope of a strain-life curve by varying the degree of misalignment achieved in processing or by comparing the cycles to kink band formation at sites that differ in misalignment.

In tensile fatigue loading, the first evident fatigue damage is matrix cracking normal to the load axis

(Section 2.2). This will be dealt with below under the constitutive properties of the effective medium. Matrix damage is followed by tow rupture. The rule of mixtures demonstrates that the increase in load in the aligned tows because of matrix cracking must be slight. More importantly, tow misalignment might be expected to introduce significant shear stresses within tows in tension just as in compression, leading to direct fatigue damage of the resin within tows [7]. This might lower tow strength if fibers suffer attrition following fragmentation of the resin. A law similar to that in compression is suggested

$$\frac{d\sigma_t^{(c)}}{dN} = -A_2(\Delta\sigma_t\phi_k)^{n_2} \quad (A_2 > 0) \tag{11}$$

where A_2 and n_2 are further empirical parameters.

Whether equations (10) and (11) are confirmed by experiments or whether tests will suggest alternative forms remains a topic of research.

4.2. *Constitutive laws for effective medium elements*

4.2.1. Elastic properties. An assembly of tow elements such as that of Fig. 10 cannot adequately model macroscopic shear stiffness, through-thickness stiffness, or Poisson's effect. The effective medium corrects these deficiencies.

One face of a typical effective medium element is outlined on the micrograph of an angle interlock composite shown in Fig. 1. It contains resin pockets and parts of tows oriented in various directions. While its elastic properties are complex in detail, those that remain after the axial stiffness of tows has been removed to tow elements can be approximated very simply in their spatial average. Choices appropriate to the interlock weaves studied in [1–3] are evaluated in [5]. For most composite properties, it is a fair approximation to assume that the effective medium is homogeneous and isotropic in the elastic regime, with properties given by rules of mixtures. Let G_f and G_r be the shear moduli and ν_f and ν_r Poisson's ratios for the fibers and resin. Then the shear modulus G_m and Poisson's ratio ν_m for the effective medium can be written

$$\frac{1}{G_m} \simeq \frac{V_f}{G_f} + \frac{1 - V_f}{G_r} \tag{12a}$$

and

$$\nu_m \simeq V_f\nu_f + (1 - V_f)\nu_r \tag{12b}$$

where, making due allowance for resin pockets and fluctuations in tow density, V_f is the volume fraction of all fibers averaged over the composite, as measured, for example, by weighing the fibers after removing the resin by acid digestion.

4.2.2. Strength. Tensile failure of effective medium elements occurs, for example, in the delamination of layers of stuffers and fillers during compression (Fig. 5) or in the formation of matrix cracks normal to the load axis under monotonic or cyclic tensile loading. The strength of an effective medium element is denoted $\sigma_m^{(c)}$. Examination of many micrographs reveals that the most important cracks form in layers of resin between tows rather than within the tows themselves†. Therefore, $\sigma_m^{(c)}$ is likely to reflect the properties of the resin. However, $\sigma_m^{(c)}$ will also depend strongly on the geometrical details of local fluctuations in tow deployment, resin porosity, etc., which are extremely difficult to measure or model. Furthermore, the grid is so coarse that the value of $\sigma_m^{(c)}$ at which matrix crack propagation occurs for a given value of the applied load is likely to depend on the element size. Therefore, $\sigma_m^{(c)}$ will usually be treated as a model-dependent, empirical parameter.

In fatigue, one might conjecture a law paralleling equations (10) and (11)

$$\frac{d\sigma_m^{(c)}}{dN} = -A_3(\Delta\sigma_m)^{n_3} \quad (A_3 > 0) \tag{13}$$

where A_3 and n_3 are empirical parameters and $\Delta\sigma_m$ is the cyclic stress amplitude in the effective medium element.

For failure in either monotonic loading or fatigue, experiments show that the fracture plane almost always either separates pairs of adjacent tows (e.g. the interfiller cracks of Fig. 7) or separate layers of tows (e.g. Fig. 5). For a model geometry such as that of Fig. 11, the relevant component of stress to be compared with $\sigma_m^{(c)}$ will accordingly lie in one of the Cartesian directions shown in Fig. 11. It should be averaged over the tow element, since computed variations within an element depend on the choice of element size.

4.2.3. Post-failure properties. After failure, an effective medium element will have no remanent strength in tension, but will continue to support load in compression. It can also bear tensile loads in directions orthogonal to the plane in which it failed. For example, the microcracks observed normal to the load axis in tension–tension fatigue diminish the axial stiffness but do not necessarily imply the delamination of stuffers and fillers in the manner depicted in Fig. 5. Thus, after failure, effective medium elements are anisotropic.

4.3. *Constitutive laws for coupling springs*

4.3.1. Coupling between tow and effective medium elements. When a tow fails, whether in axial compression or tension, stress redistribution is governed by sliding of the broken tow parallel to its axis in the vicinity of the failure site. Experimental observations suggest that sliding is Mode II displacement of a circumferential debond crack. A reasonable description of the redistribution of load is given by the shear

†Some microcracks are formed within tows when high through-thickness compaction loads are applied during processing. Such cracks have no effect on damage progression that has been observed as yet, although they could conceivably lower the critical stress for kink band formation and accelerate fatigue damage within tows.

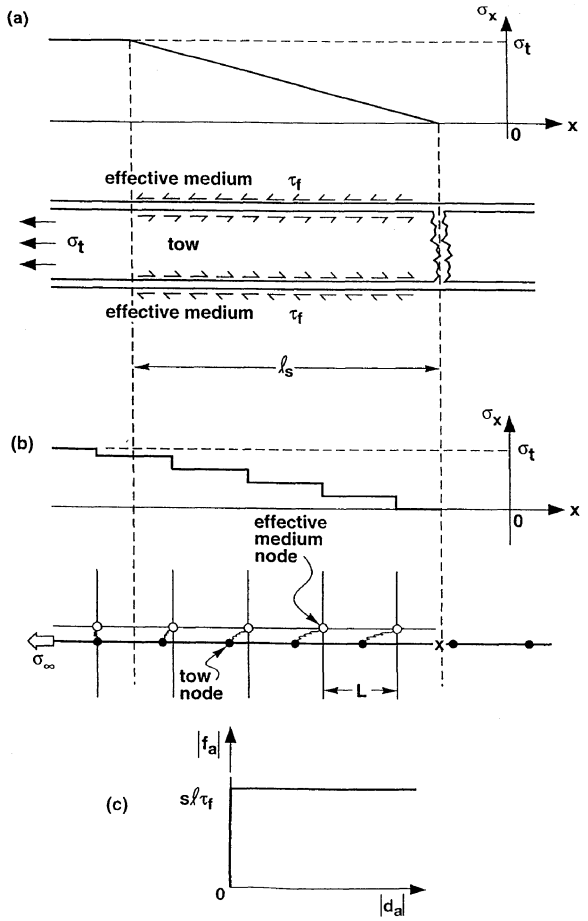

Fig. 12. (a) Shear lag depiction of stress redistribution near a site of tow failure. (b) Analog of (a) in the Binary Model. Tow and effective medium nodes have been drawn in (b) with different vertical coordinates solely to make them separately visible. Under axial loads, only their horizontal coordinates could differ in the orientation shown. (c) The constitutive law for axial displacements coupling springs between tow and effective medium elements.

lag model of Fig. 12(a). In the shear lag model, load is transferred from the tow to the surrounding composite (or "effective medium" in the binary model) via a constant frictional shear stress, τ_f, acting over the sliding boundary. The shear tractions restore the axial load, σ_x, in the tow from zero at the site of failure to the far field† value, σ_t, over characteristic length, l_s, given by force equilibrium

$$l_s = \frac{\sigma_t}{|d\sigma_x/dx|} \tag{14a}$$

$$\left|\frac{d\sigma_x}{dx}\right| = \frac{s\tau_f}{A_t} \tag{14b}$$

where s is the circumference of the tow and A_t its cross-sectional area.

†"Far field" refers here simply to the composite beyond the domain of sliding. Since the stiffness of tow elements is generally a random variable, the stresses in tow elements even in domains far removed from any stress concentrator do not share a unique value.

If the binary model is to describe stress redistribution correctly, then the gradient of axial stress in a tow near a failure site must have the value given by equation (14b), at least in its spatial average. This can be assured by appropriate specification of the constitutive laws for the nonlinear springs coupling tow and effective medium nodes. The discontinuity in the axial load in successive tow elements near the site of tow failure is simply the axial force, f_a, imposed by the coupling spring. The axial load in tow elements near the site of failure is therefore the staircase function shown schematically in Fig. 12(b). This function will have the same average gradient as $\sigma_x(x)$ in Fig. 12(a) provided

$$|f_a| = s\tau_0 L \tag{15}$$

where L is the computational element length. Equation (15) prescribes a force that is independent of the relative displacement, d_a, of the relevant tow and effective medium nodes in the axial direction, as in Fig. 12(c).

The relative axial displacement of the nodes it couples is the only degree of freedom needed for a coupling spring between a tow and the effective medium. The tow and effective medium nodes always coincide in their lateral displacements.

In the common case that τ_0 represents frictional sliding, its value should change with the transverse compression acting on the tow. The latter can be evaluated and continually updated by averaging the stress fields in adjacent effective medium elements during a simulation. In this way, the additional compressive loads introduced by warp weavers via the mechanism of Fig. 9 can be modeled.

The use of coupling springs not only provides approximately correct stress recovery in a tow near a site of failure, but also avoids physically improper behavior which would otherwise arise from the fact that tow elements have no cross section.

4.3.2. Coupling between warp weavers and fillers. In practice, the optimum combination of in-plane and through-thickness properties is usually attained in a 3D woven composite if the warp weavers are of considerably lighter denier than the stuffers or fillers and accordingly of lower volume fraction [14]. This invites the simplification of coupling warp weavers by springs directly to the fillers around which they wrap, rather than via effective medium elements, thus reducing the degrees of freedom of the model. The locations of such springs are shown in Fig. 10, while constitutive laws for them are given in Appendix C. It will be shown in [5] that this simplified treatment of warp weavers is satisfactory in the elastic regime. In modeling failure, the critical role of warp weavers is to impose lateral loads on fillers, which remains well represented.

4.4. Applications of the model

The binary scheme outlined above is potentially applicable to very diverse 2D and 3D woven and

Table 2. Specifications for the simulations of Fig. 13

k_s (Nt)	2×10^5
k_f (Nt)	1×10^5
k_{ww} (Nt)	2.5×10^4
a_x (mm)*	2
a_y (mm)*	1.8
a_z (mm)*	0.65
E_m (GPa)	10
$\langle \sigma_t^{(c)} \rangle$ (GPa)	2
$\langle \sigma_m^{(c)} \rangle$ (GPa)	∞

*See Fig. 10 for definition.

braided composites, given suitable definitions of grids and minor modifications of the constitutive laws. It is also ultimately a viable approach to modeling continuously reinforced structures, such as integrally woven or braided skin/stiffener components for airframes. Such longer term goals noted, the following examples and remarks address the subject materials of [1–4].

4.4.1. Monotonic loading. The first computer code written to solve the Binary Model was based on the ABAQUS finite element package†. Experience proved that such a package does not permit sufficient flexibility and control over the computation to enable realistic simulations in many interesting cases. Therefore, a custom finite element code was subsequently written. The new code handles all the features of the Binary Model described in this paper. It will be reported comprehensively in future papers. Here, some illustrative simulations carried out with the ABAQUS-based code are presented. They demonstrate some of the effects of introducing random strengths for tow elements and randomness in tow positioning.

The simulations were of through-the-thickness orthogonal interlock woven composites. Cartoons of the model structure are shown in Fig. 13. Warp tow elements are shown there as ribbons, faces of effective medium elements as quadrilaterals, and sections of fillers as black dots. Each simulation modeled a section of material containing ten distinct layers normal to the filler direction, which Fig. 13 shows in an exploded view. Six of the layers contain stuffers and two contain warp weavers. The ninth and tenth layers contain no warp tows; they are included to avoid tow elements (which should lie along tow axes) being present on specimen surfaces. Simulations were executed for both ideal and irregular tow positioning. Irregularity was introduced by offsetting the initial, stress-free coordinates of nodes. The offsets were chosen by Monte Carlo methods, i.e. using a pseudo-random number generator, according to an *ad hoc* random walk model. The magnitudes of the tow displacements were on average about 30% of the tow spacing in any direction.

The stiffnesses of tow elements and effective medium elements, the average tow element strength, and the element dimensions that were chosen are typical of AS4 carbon tows in an epoxy resin (Table 2). The tow elements were either assigned uniform strengths (the average $\langle \sigma_c^{(t)} \rangle$ of Table 2) or normally distributed strengths with standard deviation 20% of the average. If strengths were uniform, one centrally located element was assigned a slightly lower value than the rest, to ensure that failure started away from the specimen ends. For random strengths, the lowest strength value generated was always assigned to that same element. The effective medium was assigned infinite strength: since it is so soft, the qualitative results considered here are not greatly affected.

In these illustrative simulations, the degree of freedom that allows relative sliding of failed tow elements and the surrounding composite, as described in Section 4.3, was suppressed. (It is difficult to treat in the ABAQUS-based code.) This corresponds to the friction stress τ and therefore the stress concentration on tows neighboring a failure site both being large (but finite).

In each simulation, the applied strain was incremented in steps small enough that at most two or three and usually zero or one tow elements would fail. (Complete control is not possible in the ABAQUS-based code.) The simulations were carried on to large strains.

Figure 14 shows stress–strain records for uniaxial tension simulations under displacement control in the stuffer direction. The curves show the effect of successive tow failure events. Figure 14(a) is the case of ideal geometry and uniform tow element strengths. Brittle behavior is found: when one tow element fails, propagating stress concentration causes many tow elements to fail in an unstable manner‡. Only the stabilizing influence of the fixed grip loading conditions and the unrealistically infinite strength of the effective medium prevent total failure of the specimen. The other three cases [Fig. 14(b–d)] show the effects of irregular geometry and random strength assignments acting separately or together. Randomness in *either* geometry or strength enhances ductility.

This trend is underscored by the failure sequence of tow elements, which has been incorporated in Fig. 13 by color coding. The value of applied strain at which any tow failed is revealed by matching its color against the color strips in the inset stress–strain record.

For ideal geometry and uniform strength [Fig. 13(a)], tow failure propagates in a symmetric, deterministic way from the first failure site. Nearly all elements on the plane on which the first failure

†Hibbitt, Karlsson and Sorenson Inc., Pawtucket, Rhode Island.

‡In the ABAQUS-based code, all critically loaded elements must fail in a single load increment. For elements of *uniform strength*, this leads to multiple, simultaneous element failures along a single stuffer, as seen in Fig. 13(a), even when the load increment is very small. This unappealing and unphysical effect disappears as the distribution of tow element strengths broadens [Fig. 13(b)].

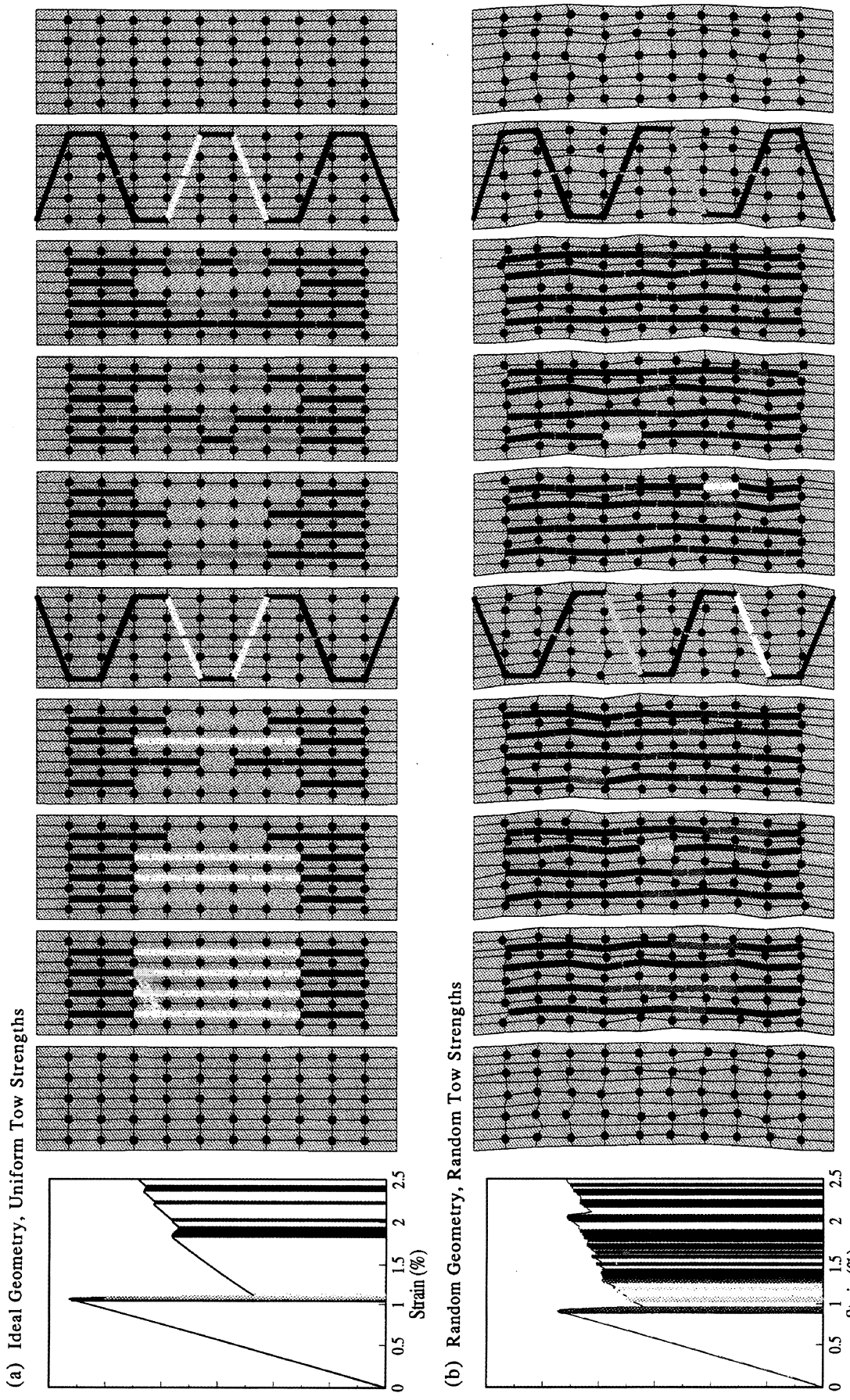

Fig. 13. Element geometry and damage sequence for orthogonal interlock composites with (a) ideal geometry and uniform tow element strengths; (b) random geometry and random tow element strengths. The inset stress–strain curves contain a color code that allows the sequence of tow failures to be mapped.

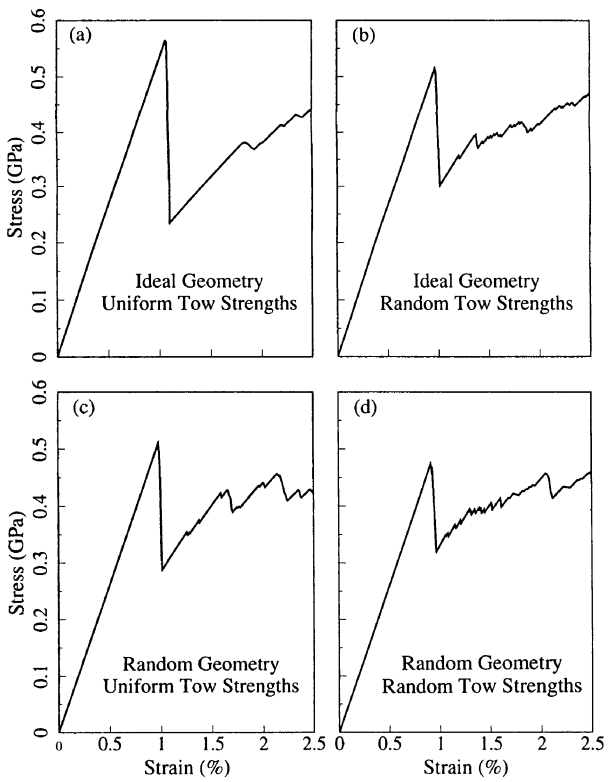

Fig. 14. Stress–strain curves for various combinations of randomness of tow strength and geometry.

occurred fail with very little increase in applied strain. Two elements survive, shielded by nearby warp weavers. A complete fracture path is still formed during the first load drop by the failure of the elements on either side of the two survivors. The propagating effects of stress concentration dominate the damage evolution.

In contrast, for the case of irregular geometry and random tow element strengths [Fig. 13(b)], half the tow elements on the plane of first failure remain intact throughout the entire process. Damage is distributed over the whole specimen, tending to occur in bursts in one distinct region after another. Randomness has induced a brittle/ductile transition.

The damage sequence when only one of geometry or strength is random appears intermediate between Fig. 13(a) and (b), as Fig. 14 and intuition would suggest. The patterns of failure found for random geometry or random strength are quite similar to one another. By increasing the variance of either initial node positions or tow element strengths, a brittle/ductile transition can be induced. Which one is the stronger factor in current 3D composites remains to be investigated.

4.4.2. Fatigue loading. Simulations of fatigue are similar in complexity to simulations of monotonic loading, but follow different constraints. Typically, either the cyclic applied load amplitude or the cyclic applied strain amplitude is specified and held constant throughout the simulation. Damage is then measured over elapsed cycles, N, treated as a continuous variable. The strength of each element decays with N according to equations (10), (11) and (13). The parameter ϕ_k is a random variable assigned an initial value for each element. The local cyclic load amplitude, $\Delta\sigma_t$ or $\Delta\sigma_m$, is computed by the model. Equations (10), (11) and (13) are integrated to identify the first element whose strength falls in fatigue to a value equal to the maximum load it bears in any load cycle. That element is then failed. The simulation is then relaxed to determined new cyclic loads on all remaining elements, which are then tested for failure without further increase in N. If none fails, equations (10), (11) and (13) are integrated again, now using the new values of local stress amplitude, until another failure is found. Ultimate failure occurs when there are sufficient failed elements to cause catastrophic damage propagation in one cycle. Quantitative examples of fatigue simulations are deferred to [6].

4.4.3. Engineering applications. As illustrated above, single simulations are executed by assigning random parameters (strengths and irregularity) with a pseudo-random number generator. The statistics of composite properties are then determined from an ensemble of simulations. Ultimately, calculations would be more efficient in a probabilistic formulation such as a Markov chain or diffusion equation. However, in this investigative phase, Monte Carlo methods have the great advantage that newly discovered phenomena are relatively easily programmed into the solution. In particular, the number of independent variables can be readily changed in a Monte Carlo simulation, whereas changing the dimension of a probabilistic formulation is a major programming exercise.

Input for the model consists of geometrical and material parameters, which either refer to deterministic quantities, e.g. average stiffnesses and lengths, or are parameters in the distributions of random variables. Some of the parameters can be regarded as known *a priori* from micromechanical arguments or measurements. Others will be empirical, having to be determined by calibrating the model against test data for the composite. A great part of current research is directed to determining which parameters fall into which category.

5. CONCLUSIONS

A Binary Model of 3D composites has been formulated in correspondence with detailed observations of failure mechanisms in angle and orthogonal interlock woven composites. Micromechanical models of local failure events and sources of elastic nonlinearity have been used to derive constitutive laws for the computational elements in the model. Emphasis is laid on the role of geometrical flaws in failure. The model has been proposed as the simplest realistic means of computing macroscopic strength, notch sensitivity and damage tolerance. Simulations of load–strain

curves and the predicted spatial distributions of tow failures are in appealing accord with experiments.

Acknowledgements—BNC and WCC gratefully acknowledge the support of NASA Langley Research Center under Contract No. NAS1-18840. In the final stages of this work, WCC was supported by internal funding at NIST. The authors are deeply indebted to Drs M. S. Dadkhah and W. L. Morris for supplying experimental context and to Drs R. M. McMeeking and J. Xu for discussions about modeling. Dr Morris also provided assistance with some calculations.

REFERENCES

1. B. N. Cox, M. S. Dadkhah, R. V. Inman and W. L. Morris, *Acta metall. mater.* **40,** 3285 (1992).
2. B. N. Cox, M. S. Dadkhah, W. L. Morris and J. G. Flintoff, *Acta metall. mater.* In press.
3. M. S. Dadkhah, W. L. Morris, S. Schroeder and B. N. Cox, *Acta metall. mater.* Submitted.
4. B. N. Cox, W. C. Carter, M. S. Dadkhah and N. A. Fleck, in *Proc. 4th NASA/DoD Advanced Composites Technology Conf.*, Salt Lake City, Utah, 1993 (edited by J. Davis and H. Bohon). NASA (1993).
5. J. Xu, B. N. Cox and M. A. McGlockton. In preparation.
6. P. W. K. Lam and M. R. Piggott, *J. Mater. Sci.* **25,** 1197 (1990).
7. M. R. Piggott and P. W. K. Lam, in ASTM-STP 1110. ASTM, Philadelphia, Pa (1991).
8. B. N. Cox and M. S. Dadkhah, *J. Comp. Mater.* Submitted.
9. A. S. Argon, in *Treatise of Materials Science and Technology*, Vol. 1. Academic Press, New York (1972).
10. B. Budiansky and N. A. Fleck, *J. Mech. Phys. Solids* **41,** 183 (1993).
11. B. Budiansky, in *Preliminary Reports, Memoranda and Technical Notes of the Materials Research Council Summer Conf.*, La Jolla, Calif. DARPA (1979).
12. M. Shuart, *Short-Wavelength Buckling and Shear Failures for Compression-Loaded Composite Laminates.* NASA TM87640 (1985).
13. B. N. Cox, in *Proc. 9th DoD/NASA/FAA Conf. on Fibrous Composites in Structural Design*, Lake Tahoe, Nevada, 1991 (edited by J. R. Soderquist, L. M. Neri and H. L. Bohon), pp. 1105–1110. U.S. Dept. Transportation (1992).
14. B. N. Cox, *J. Comp. Mater.* In press.
15. B. N. Cox, *Acta metall. mater.* **39,** 1189 (1991).
16. R. Odette, University of California at Santa Barbara, unpublished work.
17. R. Edgeson, Cambridge Consultants, Cambridge, U.K., private communication (1992).
18. D. Stover, *Adv. Composites*, July/August (1992).
19. M. Thouless and A. G. Evans, *Acta metall.* **36,** 517 (1988).
20. M. Sutcu, *Acta metall.* **37,** 651 (1989).
21. See, for example, papers in *Proc. Fourth NASA/DoD Advanced Composites Technology (ACT) Conf.*, Salt Lake City, Utah, 1993 (edited by J. Davis and H. Bohon). NASA (1993).
22. N. A. Fleck and B. Budiansky, *Proc. IUTAM Meeting*, Rennsaelar Polytechnic Institute, New York (1992).

APPENDIX A

Effective Flexural Rigidity of a Tow

Consider the problem of a tow segment of length L loaded transversely by a force of magnitude F at one end (Fig. A1).

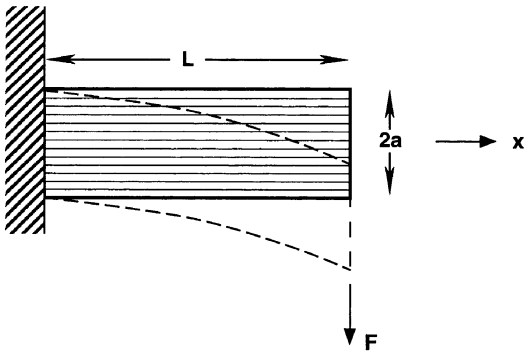

Fig. A1. Cantilever beam paradigm for estimating the proportions of bending and shear in a transversely loaded tow segment.

Suppose the other end is built in. The deflection $v_b(x)$ arising from bending satisfies

$$E_t I \frac{d^2 v_b}{dx^2} = Fx \tag{A1}$$

where E_t is the axial Young's modulus of the tow and I is the relevant moment of inertia; while that, $v_s(x)$, arising from shear satisfies

$$AG_t \frac{dv_s}{dx} = F \tag{A2}$$

where G_t is the shear modulus of the tow and A is its cross-sectional area. Hence the displacement contributions at the load point $x = 0$ are in the proportion

$$\frac{v_s(0)}{v_b(0)} = \frac{FL}{AG_t} \Big/ \frac{FL^3}{3E_t I} \tag{A3}$$

$$= \frac{3}{4}\left(\frac{a}{L}\right)^2 \frac{E_t}{G_t} \tag{A4}$$

for a tow of elliptical cross-section with semi-axis a in the direction of bending.

The axial modulus E_t can be approximated by equation (5). The shear modulus G_t can be estimated by rule of mixtures from the shear moduli G_f and G_r of the fiber and resin

$$\frac{1}{G_t} = \frac{V_t}{G_f} + \frac{1 - V_t}{G_r} \tag{A5}$$

where V_t is the volume fraction of fibers in a tow. For typical graphite/epoxy or glass/epoxy systems, the term in G_f is negligible.

The ratio E_t/G_t is typically fairly large—for AS4 graphite fibers in Shell 1895 resin, the material combination for many of the composites studied in [1–4], $V_t \simeq 0.7$, $E_f = 250$ GPa and $E_r = 3.5$ GPa, leading to $E_t \simeq 200$ GPa, $G_t \simeq 4$ GPa and $E_t/G_t \simeq 50$. Substituting this number into equation (A4) shows that shear will dominate lateral deflections of a tow segment if a force couple acts over lengths less than five tow widths.

This criterion is satisfied for forces acting on the ends of tow elements in the binary model.

APPENDIX B

Kink Band Lock Up

The relation between kink band lock up and theaxial sliding of debonded tow segments can be elucidated by simple shear lag analysis.

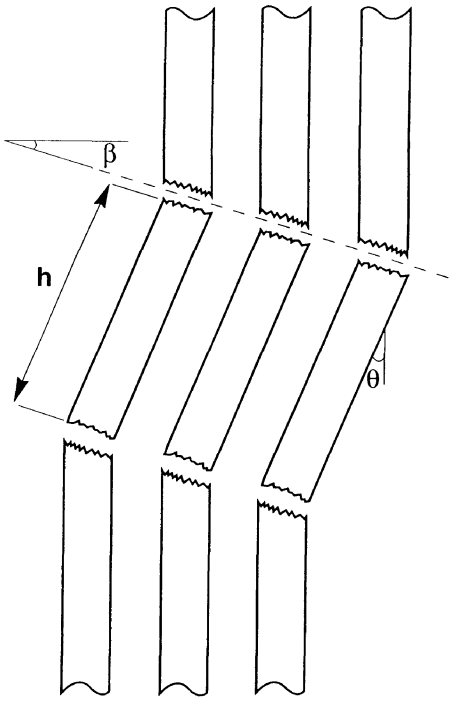

Fig. B1. Schematic of fiber rotation within a kink band.

Following formation of a kink band, the fiber segments within the band rotate (Fig. B1). At first, the rotation is accompanied by transverse dilatation. But as rotation progresses, the fibers are drawn back together. At some critical rotation angle, θ_c, the volumetric strain in the band vanishes and further rotation is very strongly resisted. The band is effectively locked up. If the boundaries of the kink band form angle β to the boundaries of the tow (Fig. B1), the condition of vanishing volumetric strain leads to [22]

$$\theta_c = 2\beta. \tag{B1}$$

Typically, $\beta = 20$–$30°$.

Assume that kinking is accompanied by debonding of the tow over a sliding length l_s and that the axial compressive stress at the kink band is zero prior to lock up. Then, according to the same shear lag model that underlies equation (19), sliding will produce an axial displacement u of the ends of each of the intact parts of the tow given by

$$u = \frac{1}{2}\frac{\sigma_t^2 A_t}{E_t s \tau_0} \tag{B2}$$

where σ_t is the stress in the tow remote from the kink band, A_t and s are the cross sectional area and circumference of the tow, and τ_0 is the critical shear stress for sliding of the tow.

If the length of fibers within the kink band is h (Fig. B1), lock up will occur when

$$u = \frac{h}{2}(1 - \cos\theta_c). \tag{B3}$$

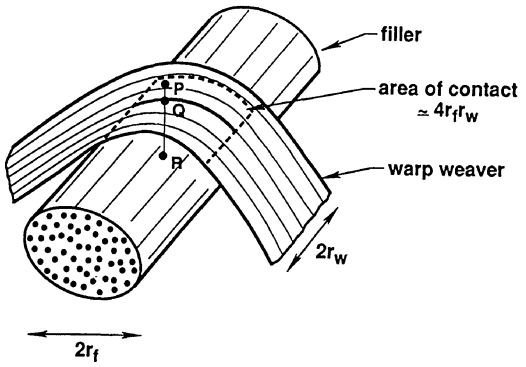

Fig. C1. Schematic of a warp weaver wrapping around a filler in an interlock weave.

The corresponding value, σ_1, of the remote stress in the tow is

$$\sigma_1 = \left[2u \cdot E_t \frac{s\tau_0}{A_t}\right]^{1/2}. \tag{B4}$$

The critical stress for lock up depends via (B3) on the kink band length, h, which is difficult to predict.

APPENDIX C

Coupling Springs Between Warp Weavers and Fillers

Figure C1 shows a schematic of a warp weaver wrapping around a filler. The warp weaver has a radius r_w and the filler a radius r_f, which can be estimated from the fiber volume fraction, V_t, within a tow ($V_t \simeq 70\%$), the denier of the tow, and the density of the fibers. In the elastic regime, displacement of the point P on the axis of the warp weaver relative to the point R on the axis of the filler is resisted by the transverse stiffness, E_{tr}, of the two tows. This might be approximated by the rule of mixtures

$$E_{tr} = [V_t/E_f + (1 - V_t)/E_r]^{-1} \tag{C1}$$

where E_f and E_r are the fiber and resin moduli. Assuming the contact area $4r_f r_w$ (Fig. C1), the effective spring constant k_{wf} coupling the warp weaver and filler is defined by

$$k_{wf} = E_{tr} \cdot 4r_f r_w \tag{C2}$$

where the spring constant relates force to proportional change in displacement. Equation (C2) can be readily generalized to the case of tows containing different kinds of fibers.

Failure of the spring occurs at some critical tensile displacement, which will usually be treated as an empirical parameter.